Chapter 5

A comparative study on the physico-mechanical properties of silica compacts fabricated using rice husk ash derived amorphous and crystalline silica

5.1. Introduction

Silicon dioxide, one of the most commonly used materials in the scientific fraternity, is found in multiple forms in nature. Silica has both amorphous and crystalline forms, with quartz, tridymite, and cristobalite as their most stable crystalline forms [1]. The potential application of silica is not limited to structural refractories; they are also widely used by the semiconductor and insulator industries and is an excellent adsorbent [2-4]. The several intrinsic properties of silica make it a suitable candidate for use as the matrix for incorporating other functional components and as a reinforced material for different matrix phases [5]. The properties like water solubility, thermal stability, chemical and magnetic field inertness, excellent biocompatibility, and cheap availability give silica an extra edge toward being used for various applications [6]. Composites developed with the help of silica as a matrix or reinforcement phase possess unique mechanical, thermal, magnetic, optical, and electric properties [7]. Silica-based materials are also found in advanced applications like radome [8]. Apart from dense silica, porous silica has been widely used in various applications [9-12]. Fu et al. have successfully utilized a porous silica-based composite to remove phosphorus [9]. Similarly, Kobayashi studied the effect of porous silica on removing tar components and found it to be very efficient [11]. Wu et al. have shown good adsorption and separation behavior of porous silica towards Y(III) and Sr (II) in acid solution [10]. Silica, mostly available as quartz in the silica sand, is the cheapest source of silica; it is also found in various rocks in tridymite and cristobalite forms. However, some other typical chemical routes can be used to synthesize silica. In the past few decades, silica from Rice Husk (RH) and agricultural waste has emerged as the cheapest source of silica [13]. Amorphous and crystalline silica forms are available through RH under suitable conditions [14].

Millions of tons of rice are produced globally per annum. According to the literature, around 200 kg of Rice Husk (RH) is produced per metric ton of rice [15]. Disposal of RH is a great challenge associated with rice production due to its large surface area and carbon content, causing a pollution threat to the environment. Efforts have been made to utilize RH properly without affecting the environment. Some researchers used RH directly to reinforce it with other components, while most of them have used it as ash to utilize its high silica content [16]. Hydrated Silicon, cellulose, and lignin are the major constituents of Rice husk [17]. Various approaches, including chemical and thermal treatment, have been used to synthesize silica from RH [18]. However, thermal treatment is the most preferred one. The silica produced requires minimum grinding due to the highly reactive nature of silica particles, which can be considered the main advantage of this process. Carbonaceous constituents of the rice husk provide the energy required for its pyrolysis, which produces highly porous silica with a large surface area [19]. During the whole process, 20 wt.% of rice husk remains as the burnt-out residue, of which 95 wt.% contains silica. It has been studied earlier that the quality of silica produced from rice husk ash depends on sintering temperature and time. These sintering conditions are also responsible for the structural transformation of silica [20]. RH sintered at a lower temperature of 800°C produces amorphous silica, and crystalline silica is found above 900°C [21]. The most widely recognized types of crystalline silica are quartz and cristobalite. The tridymite phase may also be evident in some cases, depending on the percentage of impurity content in RHA [22]. Many studies have demonstrated the efficiency of using RHA-based silica precursors for ceramic/metal/polymer-based composite production in order to improve their mechanical properties [23-25]. Santos et al. investigated the effect of RHA-kaolin-based composite reinforced with corrugated steel fibers [26]. The results showed that the composite has a high degree of deformation at the

point of rupture and better thermal shock resistance. The effect of reactive silica from RHA has been investigated on the mechanical and microstructural properties of metakaolin/volcanic ash-based geopolymer [27]. The higher mechanical strength of geopolymer is obtained due to the enhanced compactness provided by RHA silica. Mechanical and wear behavior is analyzed on aluminum composites using alumina, RHA, and graphite as reinforcement, and it found that tensile strength becomes higher when 50% RHA is used [28]. Similarly, the effect of RHA silica reinforcement on copper matrix and their wear behavior is analyzed by Dinaharan et al., who found a decreased wear rate of Cu/RHA composite [29]. The role of RHA silica on polymer-based composites is also widely studied. Ayswarya et al. studied the role of RHA on epoxy composites and found that nano-silica obtained from RHA gives better tensile strength and thermal stability to epoxy composites [30]. RHA-based silica is also used to fabricate a variety of silicate ceramics and silicon-based non-oxide ceramics like SiC and Si_3N_4 [31,32]. The above investigations provide enough evidence on the use of RHA-based silica with different materials, showing its importance in improving the mechanical and other properties of metal/ceramic/polymer-based composites. Both amorphous and crystalline forms of silica are available through RHA. Researchers have extensively used these forms of silica to get anticipated results. However, none of the research has focused on the selective study of these two different forms of RHA-based silica or their composites. Thus, we herein report a systematic study on the various available forms of silica obtained through the thermal treatment of RH, including their microstructural and mechanical properties. Thermal treatment of RH has been carried out in various forms. Four different temperatures treated RHA silica, both of amorphous and crystalline form, is used to fabricate silica compacts. Sintering is done between 1450°C-1550°C for the final consolidation of silica compacts. Effects of silica structure and phase percentage on compaction behavior, green density,

sintered density, microstructure, and mechanical properties have been analyzed. XRD and SEM analyses are used to study different silica phases and their microstructure, respectively. Finally, a comparative analysis of these forms on silica compacts' mechanical and microstructural properties has been conducted.

5.2. Experimental

5.2.1 Materials

Rice husk has been collected from a local agricultural farm. The obtained RH has been treated with normal tap water and deionized (DI) water to completely remove any dust particles and soil contents. Washed RH is dried in the oven at 110°C for 10 hrs. Sucrose (Merck, India) and DI used are analytical grades. Sucrose is used as a binder material and prepared by mixing sucrose and DI in a 1:1 proportion.

5.2.2 Silica Compact Fabrication

Washed and dried RH was heat-treated at different temperatures ranging from 100°C to 1200°C to obtain RHA. These RHA were then mixed and granulated in the mortar pestle to get RHA powder. After XRD analysis, these RHA powders were separated into amorphous RHA and crystalline RHA. Silica compacts were prepared using both amorphous and crystalline RHA powder. The dry pressing method is used to prepare pellets using a hydraulic press with a load of 10 tons. An optimized amount of binder solution is mixed with each powder before pressing. A mould with a diameter of 15mm is used to prepare all the samples. Obtained silica pallets are sintered at different temperatures with a heating rate of 5°C/min and a soaking time of 2 hrs.

5.2.3 Characterization and Mechanical Analysis

To examine the nature of RHA, XRD measurements are carried out using an X'Pert Pro

diffractometer equipped with Cu-kα (1.5406 Å) radiation as the X-ray source, in the 2θ range of 10-110° with a step size of 0.02°. The surface microstructure analyses have been carried out with the help of a Scanning Electron Microscope (SEM) (ZEISS, Jena, Germany, EVO 18-2045). Elemental percentage in each type of RHA was determined using EDX analysis. The Archimedes method determined Porosity and bulk density according to ASTM C 20. The compressive strength of sintered samples is calculated as per ASTM C133-97(2021) standard using a Universal Testing Machine (AGS-5KND, P/N 340-33309) with a crosshead speed of 0.2 mm/min. Dynamic light scattering (Model no: Malvern ZETASIZER Nano S90) was used to measure the average particle sizes of the different temperature calcined RHA powders. The surface area of RHA particles was measured using BET (BELLSORP MAX II & BELCAT-II, MicrotracBEL Corp.) analysis.

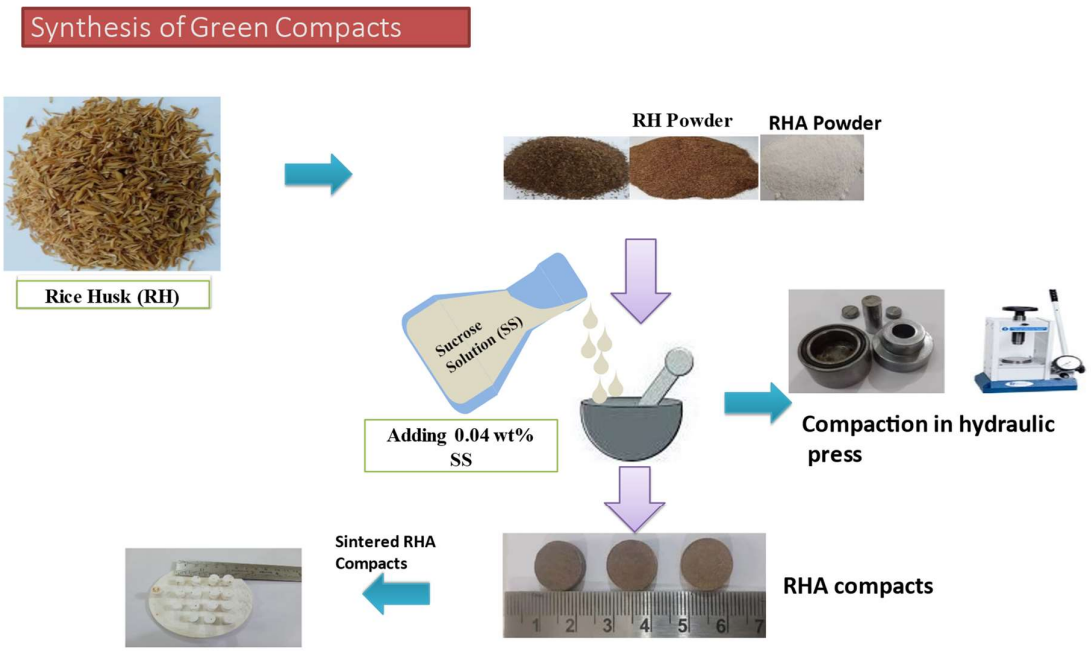

Figure. 5.1. Synthesis of Rice Husk Ash (RHA) sample.

5.3 Results and Discussion

5.3.1- Physical and Microstructural analysis of heat-treated RHA powder

Figure. 5.2. Effect of temperature on the physical appearance of Rice Husk (RH).

The washed RH are heat-treated at different temperatures ranging from 100°C to 1200°C. Fig. 1 shows the change in the physical appearance of RH with the increase in temperature. Initial heat treatment up to 300°C turns RH into dark black material due to water content loss and cellulose and lignin decomposition, which triggers carbonization. Above 300°C, due to the oxidation of carbonaceous phases, the black-colored RH now turns to pale yellow. This change in physical appearance remains silent for further heating with little change in color from pale yellow to snow white. This might be due to differences in phases and their concentration. These results are well supported by the TGA graph (Fig. 5.3). Around 19.6 % of burnt-out residue in the form of RHA is obtained during heat treatment of RH. TGA analysis of RH shows weight loss during thermal treatment of RH in air, which occurs in three stages [33]. The first stage corresponds to drying (50-200°C) to remove physically bonded water, which corresponds to 0.99 wt.% loss of the original mass. The second stage belongs to the burnout of volatile organic components with 64.89 wt.%. Loss (200-340°C), and the final stage is due to the degradation of carbonaceous phases, cellulose, and hemicellulose (14.51 wt.% loss) (340-500°C), leading to a total cumulative weight loss of 80.39 wt.%.

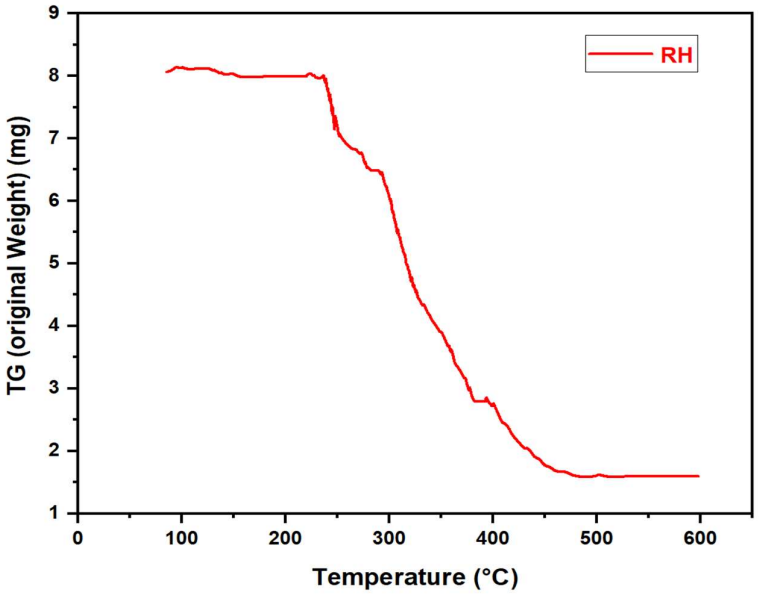

Figure. 5.3. Thermogravimetric analysis (TGA) graph showing weight loss of Rice Husk (RH) with temperature.

The XRD pattern of RHA, treated at various temperatures, is shown in Fig.3. Silica is the main constituent of RHA, as evident from the XRD pattern and literature reviews [34]. The XRD pattern shows the amorphous nature of RHA up to 700°C. Peaks start appearing from 800°C onwards, showing the transformation of amorphous silica into crystalline silica. XRD displays fractional crystallization after presentation at 800°C for two hours and experiences total change at 900°C for two hours. The crystalline state is comprised of two phases: cristobalite and tridymite. Intensities of the crystalline peak increase with burning temperature and begin around 900°C. The peak intensities become more pronounced after increasing the heating temperature. Sharp peaks, around 20.60°, 21.82°, 27.47°, 31.30°, 36.05°, 44.53°, 46.75°, 48.49°, 57.01°, and 60.05°, are displayed in this figure and are of cristobalite and tridymite phases of silica. Peaks at 20.60°, 27.47°, 46.75°, and 48.49° belong to the tridymite phase (JCPDS no. 16-0152), while the remaining peaks are of the cristobalite phase (JCPDS no 77-1317). It is also clear from the XRD pattern that cristobalite is the main phase of the obtained silica, as most of the peaks

matched with cristobalite.

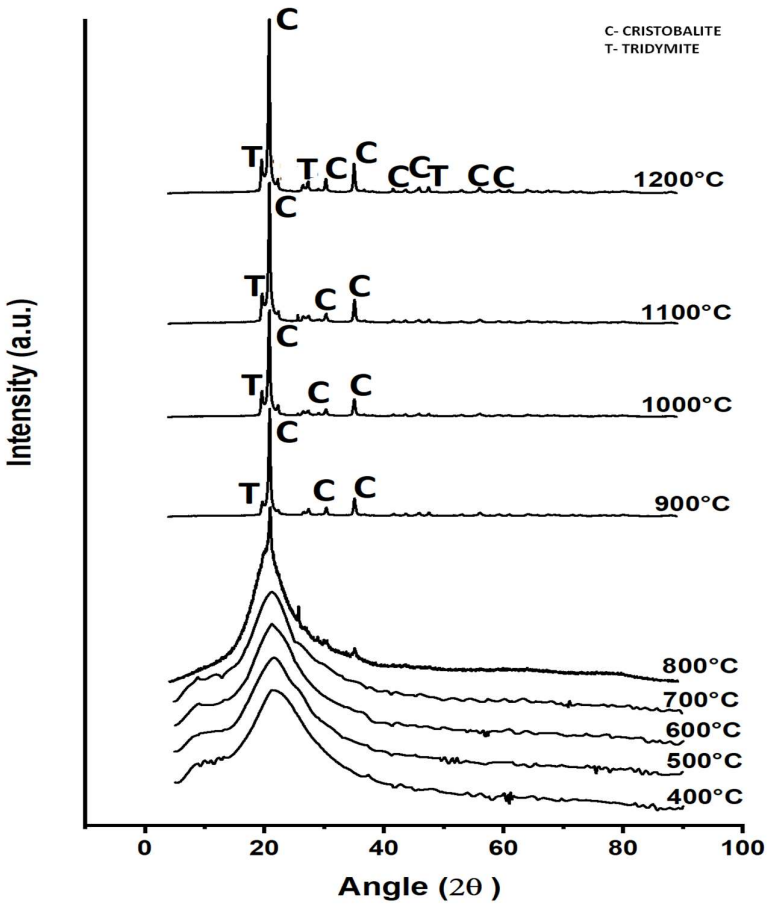

Figure. 5.4. X-ray diffraction (XRD) pattern of heat-treated Rice Husk Ash (RHA) at different temperatures.

5.3.2- Density and strength of green silica compacts

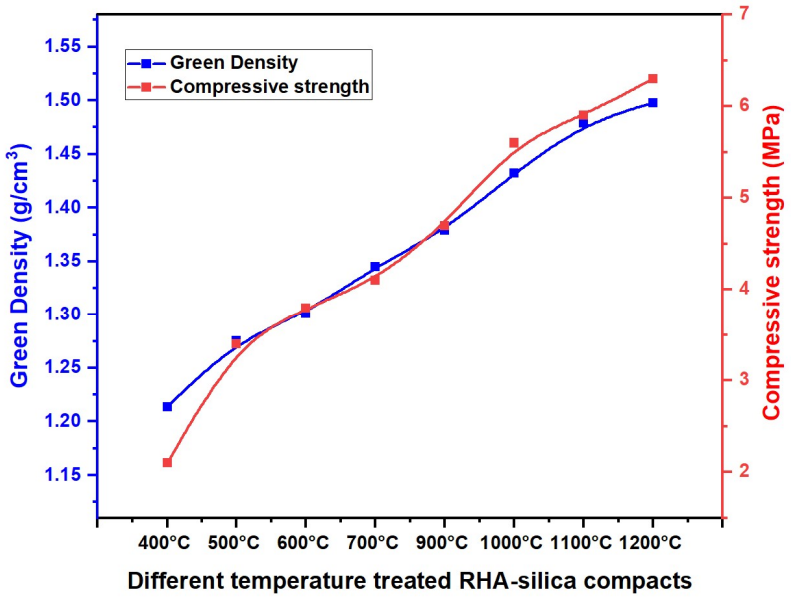

Figure. 5.5. Green properties of silica compacts fabricated using different heat-treated Rice Husk Ash (RHA).

Green density is measured for all the samples using the mass-by-volume method. Fig. 5.5 shows the variations in green densities of samples prepared using the amorphous and crystalline forms of RHA treated at different temperatures. Samples prepared using an amorphous form of RHA show lesser green density than samples prepared using crystalline silica. This trend is attributed to the well-defined and arranged structure of the crystalline form compared to the amorphous form, which helps the crystalline form in proper packing and, hence, in better densification. Due to the disorganized nature of the amorphous form, packing density is low. Also, particle size and specific surface area of RHA powders obtained using DLS and BET analysis reveal that amorphous RHA powders are finer and have a more specific surface area than crystalline RHA (Table 5.1). Finer particles are more

likely to agglomerate, so the green density of silica compacts prepared using amorphous RHA is lower than that of crystalline RHA, which has coarser particles. Another factor influencing green densification is the particle size distribution of powders being used for fabrication. Powders with narrow size distribution lead to lower packing density and, hence, lower green density. On the other hand, powders with a wide size distribution lead to improved packing and, hence, higher green density. Generally, amorphous powders have a narrow size distribution compared with crystalline powders and thus have lower green density. SEM micrograph (Figure. 5.6 (c, d)) reveals that crystalline silica possesses different-sized particles. Moreover, RHA calcined at higher temperatures contains many crystalline powders due to better conversion at higher temperatures. So, silica compacts prepared using higher-temperature calcined RHA powders show high green density compared to samples prepared using lower-temperature calcined RHA. The above explanation is well supported by the SEM microstructure of green silica samples (Fig. 5.6).

Table 5.1: Average particle size and specific surface area of different temperature calcined Rice Husk Ash (RHA).

S.No.	RHA calcined at different temperatures	Nature	Average particle size (nm)	BET surface area (m^2/g)
1	RHA-500	Amorphous	552	72.965
2	RHA-700	Amorphous	721	12.623
3	RHA-1000	Crystalline	1005	0.258
4	RHA-1200	Crystalline	1212	0.3177

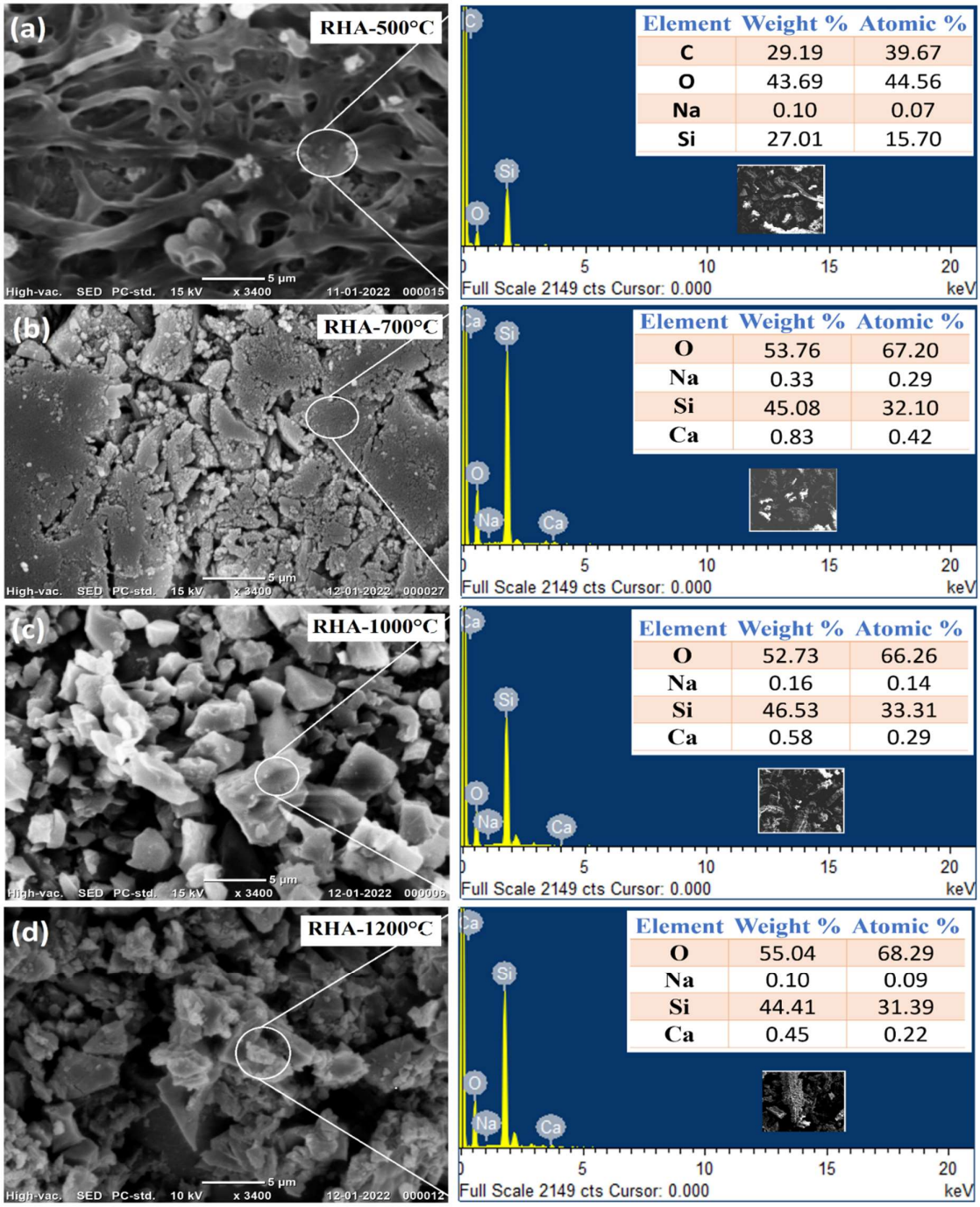

Figure. 5.6. Scanning Electron Microscope (SEM) microstructure and Energy Dispersion X-ray Analysis (EDX) data of green silica compacts fabricated using different heat-treated Rice Husk Ash (RHA).

SEM micrograph of fractured green compacts of 500°C-treated RHA shows the fibrous structure (Figure 5.6 (a)). The fibrous nature of RHA deteriorates during compaction due to pressing and results in less-dense silica compacts. Samples prepared using 700°C treated

RHA show better densification than the previous one due to the obsoleted fibrous structure (Fig. 5.6- (b)). Still, these compacts have less density compared to samples prepared using higher heat-treated RHA. This could be related to the amorphous nature of RHA. Grains are easily seen in SEM images of samples prepared through 1000°C and 1200°C treated RHA (Fig. 5.6- (c)). These grains are associated with the crystallinity of RHA powder when heat-treated above 900°C, as revealed by the XRD pattern. Silica compacts achieve better green density due to these grains (Fig. 5.6- (d)). A similar trend is observed for compressive strength. Silica compacts prepared using crystalline RHA have higher compressive strength compared to amorphous silica due to better densification. The compressive strength of green silica compacts lies in the range of 2.1 MPa to 6.3 MPa.

5.3.3- Microstructural and Mechanical strength analysis of sintered silica compacts

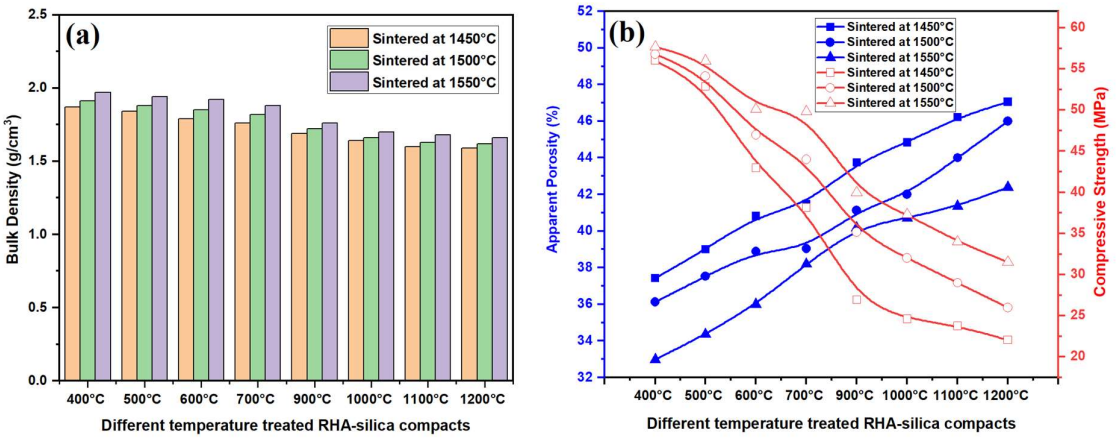

Figure. 5.7. Physical and mechanical properties of sintered silica compacts fabricated using different heat-treated Rice Husk Ash (RHA).

Silica compacts are successfully fabricated using different heat-treated amorphous and crystalline RHA and an optimized amount of sucrose binder solution. These samples are further sintered at three temperatures (1450°C, 1500°C, and 1550°C) for final consolidation. The bulk density of the obtained samples is in the range of 1.59-1.97 g/cm^3

(Fig.5.7). Samples sintered at higher temperatures show more bulk density for all types of RHA. This could be understood by better consolidation of samples at higher temperatures. A decreasing trend is observed in the bulk density of silica compacts with higher-temperature treated RHA. The fabricated samples surprisingly show a reversing trend in densification and mechanical strength as compared with green samples. The sintered samples prepared using amorphous RHA show better bulk density, irrespective of the fact that the green density of amorphous samples is lower than that of samples prepared using crystalline RHA. The authors believe this trend is associated with the percentage concentration of silica phases and conversion rate.

The kinetics of crystallization of amorphous silica to cristobalite involves three stages. In the first stage, nucleation will occur with the subsequent growth of future crystallization centers. The above stage is critically dependent on temperature and oxidation time during heating, i.e., at a lower temperature, soaking time is required to get the same percentage of cristobalite phase when treated at a higher temperature with less soaking time. Also, the above stage is accelerated by impurities, e.g., Na. In the second stage, crystal growth will increase in the crystallization centers when the nuclei reach a critical size. Finally, an equilibrium phase will be established [35]. Thus, from the above mechanism, it can be concluded that when amorphous RHA is heated continuously at higher temperatures, there is a higher probability of conversion of amorphous RHA into the cristobalite phase by surpassing the intermediate tridymite phase. Since RHA contains sodium (Na), it also helps accelerate the conversion of cristobalite from the amorphous phase.

RHA calcined at higher temperatures contains a sufficient amount of tridymite phase along with cristobalite phase. Silica compacts are prepared using these RHA when sintered at higher sintering temperatures, and the conversion of tridymite to cristobalite

occurs. This conversion is slower than amorphous RHA and cristobalite conversion. Also, impurities like CaO inhibit this conversion or make the tridymite phase stable at higher temperatures [36]. Thus, these combined mechanism decreases the cristobalite percentage in the final silica compacts when prepared using higher temperature calcined RHA. Apart from the above reason, two more explanations that influence the densification process of silica compacts prepared using amorphous and crystalline RHA are explained below:

1- *Viscous effect- The sintering* process in amorphous material refers to viscous sintering, where matter transport occurs predominantly by viscous flow. Viscosity decreases with increasing sintering temperatures, and it also decreases with increasing impurities. Also, densification is high in less viscous materials. The crystalline phase has a considerably higher viscosity than the amorphous phase, and thus, densification decreases [37].

2- *Particle size*- The most important driving force for sintering is the curvature of the particle surface [32]. The finer the particles, the higher the curvature, and the better the sinterability. Since amorphous RHA is finer compared to crystalline RHA (obtained using the DLS method), sinterability and so densification are better in silica compacts prepared using amorphous RHA.

Volumetric expansion and compression are seen in silica due to phase change when it undergoes thermal treatment [38]. Silica mainly consists of cristobalite and tridymite phases above 1000°C. According to the silica phase diagram, the tridymite phase is the main phase of silica up to 1470°C, which converts to cristobalite beyond this temperature till the melting point. Many researchers have also reported that the cristobalite phase appeared before 1470°C in RHA-based silica [39]. Inversion of tridymite and its stability are associated with impurities like CaO, i.e., higher impurities lead to a higher concentration of tridymite phase, even at a temperature above 1470°C. Since RHA has

these types of impurities to some extent (revealed by many researchers through XRF), the tridymite phase also appears beyond 1470°C in RHA silica compacts. So, both tridymite and cristobalite phases are present in RHA silica compacts with varying concentrations between 1000°C-1550°C. Their amount in silica decides the overall calculated density of

Table 5.2

Details of the structural parameters obtained from X' pert High Score Software.

Sample	Sintering temperature (°C)	Phase	Semiquantitative concentration (weight %)	Crystal system	Calculate density (gm/cm^3)	Lattice parameter (a, b, c) (Å)	Average Crystallite size (Å)	RIR	Reference code
RHA-500	1450	Cristobalite	54	Tetragonal	2.34	4.964, 4.964, 6.92	106.167	4.77	75-0923
		Tridymite	46	Monoclinic	2.26	18.524,5.003,23.81	113.333	1.37	76-0894
RHA-500	1500	Cristobalite	55	Tetragonal	2.41	4,9226,4.9226,6.8173	291.167	4.38	82-1406
		Tridymite	45	Anorthic	2.28	9.9320,17.2160,81.8640	345.5	1.37	71-0261
RHA-500	1550	Cristobalite	69	Tetragonal	2.34	4.964, 4.964, 6.92	296	5.23	75-0923
		Tridymite	31	Monoclinic	2.26	18.524,5.003,23.81	325.667	1.37	76-0894
RHA-700	1450	Cristobalite	51	Tetragonal	2.33	4.9717,4.9717,6.9223	298	5.00	82-1232
		Tridymite	49	Anorthic	2.28	9.9320, 17.2160, 81.8640	471.833	1.37	71-0261
RHA-700	1500	Cristobalite	56	Tetragonal	2.33	4.9717,4.9717,6.9223	367.833	5.00	82-1232
		Tridymite	44	Anorthic	2.28	9.9320, 17.2160, 81.8640	222.167	1.37	71-0261
RHA-700	1550	Cristobalite	62	Tetragonal	2.33	4.9717,4.9717,6.9223	409.5	4.91	77-1316
		Tridymite	38	Anorthic	2.28	9.9320, 17.2160, 81.8640	669.667	1.37	71-0261
RHA-1000	1450	Cristobalite	47	Tetragonal	2.33	4.9717,4.9717,6.9223	256.5	5.00	82-1232
		Tridymite	53	Anorthic	2.28	9.9320, 17.2160, 81.8640	109.667	1.37	71-0261

RHA-1000	1500	Cristobalite	53	Tetragonal	2.33	4.9717,4.9717,6.9223	319.83	5.00	82-1232
		Tridymite	47	Anorthic	2.28	9.9320, 17.2160, 81.8640	362.5	1.37	71-0261
RHA-1000	1550	Cristobalite	61	Tetragonal	2.33	4.9717,4.9717,6.9223	323	4.91	77-1316
		Tridymite	39	Anorthic	2.28	9.9320, 17.2160, 81.8640	322	1.37	71-0261
RHA-1200	1450	Cristobalite	38	Tetragonal	2.33	4.9717,4.9717,6.9223	306	5.00	82-1232
		Tridymite	62	Anorthic	2.28	9.9320, 17.2160, 81.8640	304.333	1.37	71-0261
RHA-1200	1500	Cristobalite	42	Tetragonal	2.33	4.9717,4.9717,6.9223	300.833	5.00	82-1232
		Tridymite	58	Anorthic	2.28	9.9320, 17.2160, 81.8640	357.5	1.37	71-0261
RHA-1200	1550	Cristobalite	52	Tetragonal	2.34	4.964,4.964,6.9200	408.5	5.23	75-0923
		Tridymite	48	Anorthic	2.28	9.9320, 17.2160, 81.8640	404	1.37	71-0261

silica, which further affects the bulk density of compacts

The X' pert high score plus software is employed to determine the percentage proportion of the phases in the silica compacts. Table 2 provides the detail of the Semiquantitative concentration of different phases with their crystal system information was fabricated using different heat-treated RHA. Table 2 also provides details of the average calculated density and average crystallite size of silica compacts. It is clear from Table 2 data that the formation of the cristobalite phase is more in silica compacts fabricated using amorphous RHA. The XRD pattern can also confirm this, as shown in Fig. 5.8. Silica compacts prepared using amorphous RHA show higher bulk density due to the higher cristobalite content. At higher sintering temperatures, the amorphous silica compacts directly convert to the cristobalite phase, surpassing the tridymite phase. The formation of the tridymite phase is also evident due to impurities, but the amount of this conversion is low. But when silica compacts fabricated using the crystalline phase are sintered at higher temperatures, silica follows the tridymite to cristobalite conversion stage. Since crystalline

RHA already has tridymite as its main phase, the conversion from tridymite to cristobalite at a higher temperature is a little slow. Thus, silica compacts fabricated with crystalline RHA have a lesser cristobalite phase at higher temperatures, making it less dense.

The silica compacts show more bulk density when sintered at higher temperatures for all samples, whether prepared through amorphous RHA or crystalline RHA. This phenomenon may be attributed to the better conversion of the tridymite phase to the cristobalite phase at higher temperatures. The above fact is well supported by the XRD pattern (Fig. 5.8), which clearly shows the lesser intensity of the tridymite phase at higher temperatures. Fig. 5.9 represents SEM micrographs of polished and silica compacts fabricated using amorphous and crystalline RHA and sintered at different temperatures. Samples prepared using amorphous RHA, when sintered at higher temperatures, show better compaction as revealed by SEM microstructure. The authors believe that the above facts can also be correlated to the lesser green density of silica prepared using amorphous RHA. When sintered at higher temperatures, these less-dense samples undergo crystal formation. Because of more space due to low densification, these crystals rearrange themselves in better compact arrangements, thus making sintered samples more densified. The densification becomes better when the sintering temperature increases, as revealed in SEM micrographs (Fig.5.9).

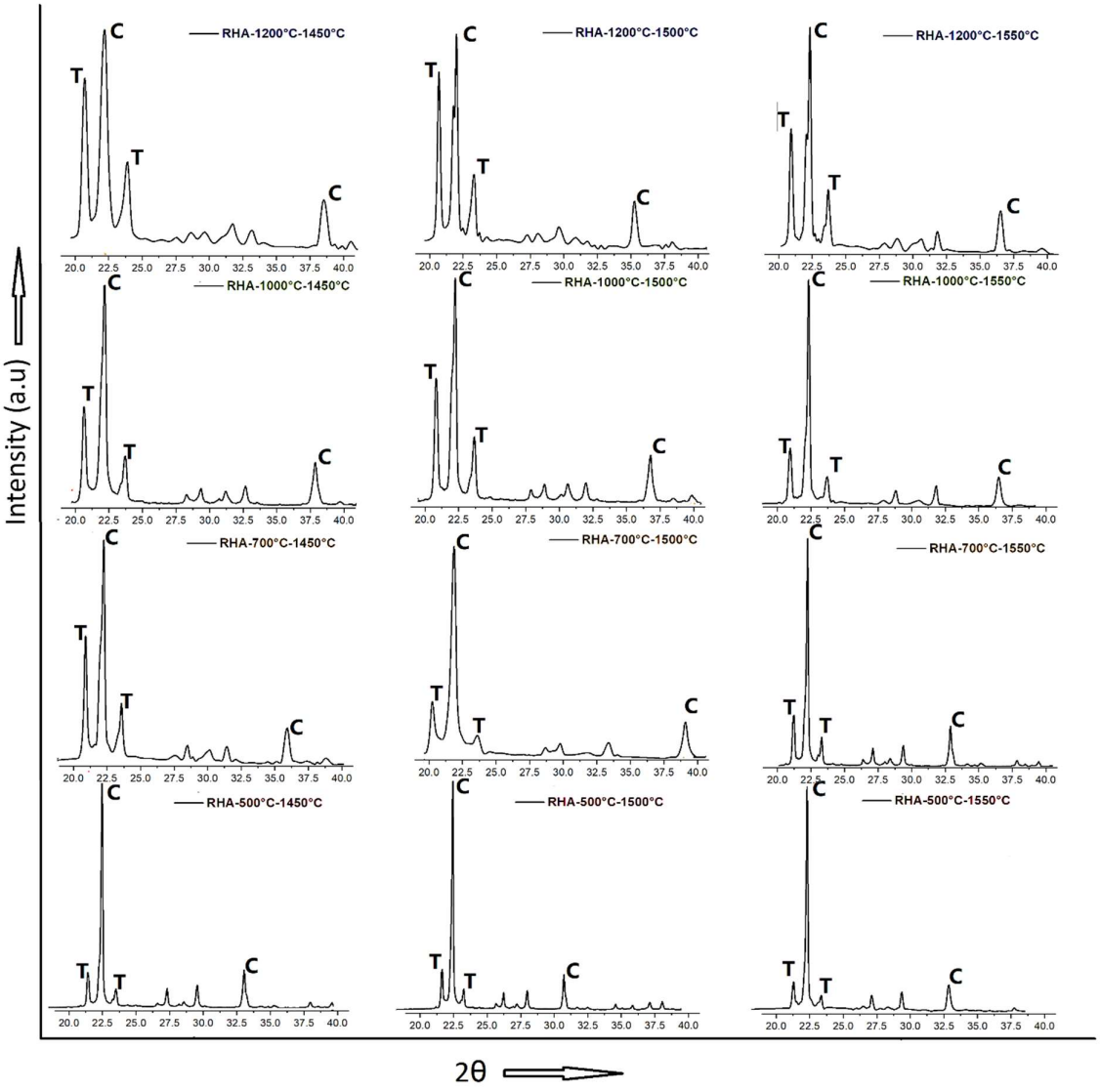

Figure. 5.8. X-ray diffraction (XRD) pattern of silica compacts fabricated with different heat-treated Rice Husk Ash (RHA) and sintered at various temperatures.

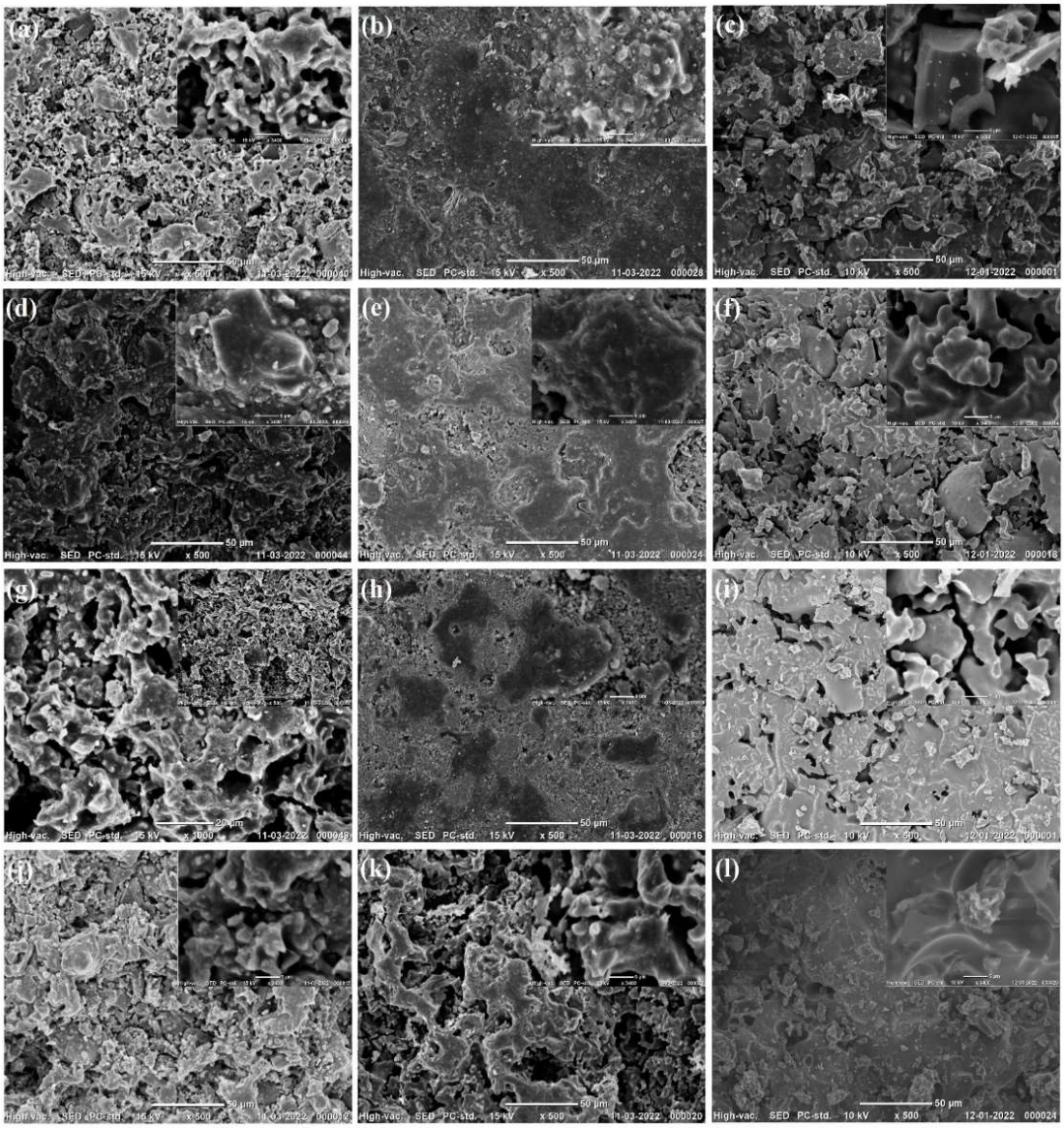

Figure. 5.9. Scanning Electron Microscope (SEM) microstructure of sintered silica compacts fabricated using different heat-treated Rice Husk Ash (RHA).

500°C treated RHA sintered at

(a)-1450°C

(b)-1500°C

(c)-1550°C

700°C treated RHA sintered at

(d)-1450°C,

(e)-1500°C,

(f)-1550°C

1000°C treated RHA sintered at

(g)-1450°C,

(h)-1500°C,

(i)-1550°C

1200°C treated RHA sintered at

(j)-1450°C,

(k)-1500°C,

(l)-1550°C.

5.4 Conclusion

It can be concluded that

1. Silica compacts were successfully fabricated using RHA and sucrose (binder). RH is treated at various temperatures and characterized by XRD to understand the RHA's physical and structural changes with temperature.

2. RHA silica is in the amorphous form up to 800°C, which ultimately converts to crystalline after 900°C. The temperature interval between 800°C-900°C is the conversion stage in which RHA silica transforms from amorphous to crystalline.

3. Phases concentration varied for each temperature range. The cristobalite phase is the main dominant phase at higher temperatures, with some traces of tridymite. Tridymite concentration is dependent on the quantity of impurities like CaO in RHA.

4. Tridymite to cristobalite inversion occurs at 1470°C. But here, instead of transitioning from tridymite to cristobalite conversion, RHA directly undergoes phase transformation to cristobalite. Four different temperature-treated RHA of each amorphous and crystalline form are taken for fabrication.

5. The obtained silica compacts possess bulk density and compressive strength in the range of 1.59 g/cm3- 1.97 g/cm3 and 20 MPa- 52 MPa, respectively.

6. Samples prepared using amorphous silica show a lower green density than crystalline silica samples. It is because of the proper compaction of a crystalline form.

7. The sintered densities and mechanical properties of samples prepared using amorphous powder are better than those of crystalline powder samples.

8. Amorphous RHA obtained at lower temperatures is better used to make silica compact for better strength. Still, crystalline RHA at higher temperatures is the preferred one if porosity is a concern.

References

[1] M. del C. Gutiérrez-Castorena, W.R. Effland, Pedogenic and Biogenic Siliceous Features, Interpret. Micromorphol. Featur. Soils Regoliths. (2010) 471–496. https://doi.org/10.1016/B978-0-444-53156-8.00021-0.

[2] G. Almarahle, Production of silica refractory bricks from white Sand, American Journal of Applied Science, 2(1): 465-468,2015.

[3] U. Nurbaiti, Darminto, Triwikantoro, M. Zainuri, S. Pratapa, Synthesis and characterization of silica sand-derived nano-forsterite ceramics, Ceram. Int. 44 (2018) 5543–5549. https://doi.org/10.1016/j.ceramint.2017.12.198.

[4] X. Tang, Y. Yu, Preparation of fumed silica compacts for thermal insulation using wet processing method, Int. J. Appl. Ceram. Technol. 15 (2018) 232–236. https://doi.org/10.1111/ijac.12791.

[5] B. Mysen, P. Richet, Chapter 5 - Silica, 2019. https://doi.org/10.1016/B978-0-444-63708-6.00005-3.

[6] K. Albert, X.C. Huang, H.Y. Hsu, Bio-templated silica composites for next-generation biomedical applications, Adv. Colloid Interface Sci. 249 (2017) 272–289. https://doi.org/10.1016/j.cis.2017.04.011.

[7] T. Ahmad, O. Mamat, R. Ahmad, Studying the Effects of Adding Silica Sand Nanoparticles on Epoxy Based Composites, J. Nanoparticles. 2013 (2013) 1–5. https://doi.org/10.1155/2013/603069.

[8] A. Nag, R.R. Rao, P.K. Panda, High temperature ceramic radomes (HTCR) – A review, Ceram. Int. 47 (2021) 20793–20806. https://doi.org/10.1016/j.ceramint.2021.04.203.

[9] F. Wu, Q. Yu, F. Gauvin, H.J.H. Brouwers, A facile manufacture of highly adsorptive aggregates using steel slag and porous expanded silica for phosphorus removal, Resour. Conserv. Recycl. 166 (2021) 105238. https://doi.org/10.1016/j.resconrec.2020.105238.

[10] H. Wu, T. Kawamura, S.Y. Kim, Adsorption and separation behaviors of Y(III) and Sr(II) in acid solution by a porous silica based adsorbent, Nucl. Eng. Technol. (2021). https://doi.org/10.1016/j.net.2021.04.009.

[11] J. Kobayashi, K. Kawamoto, N. Kobayashi, Effect of porous silica on the removal of tar components generated from waste biomass during catalytic reforming, Fuel Process. Technol. 194 (2019) 106104. https://doi.org/10.1016/j.fuproc.2019.05.027.

[12] E.N. Silva, M. Cantillo-Castrillon, T.M. Dantas, Y.M. Mesquita, D.A.S. Maia, M. Bastos-Neto, W.M. Barcellos, D.C.S. Azevedo, Siloxane adsorption by porous silica

synthesized from residual sand of wastewater treatment, J. Environ. Chem. Eng. 9 (2021). https://doi.org/10.1016/j.jece.2020.104805.

[13] E. Elimbinzi, S.S. Nyandoro, E.B. Mubofu, J.C. Manayil, A.F. Lee, K. Wilson, Valorization of rice husk silica waste: Organo-amine functionalized castor oil templated mesoporous silicas for biofuels synthesis, Microporous Mesoporous Mater. 294 (2020). https://doi.org/10.1016/j.micromeso.2019.109868.

[14] N.S. Zainal, Z. Mohamad, M.S. Mustapa, N.A. Badarulzaman, A.Z. Zulkifli, The ability of crystalline and amorphous silica from rice husk ash to perform quality hardness for ceramic water filtration membrane, Int. J. Integr. Eng. 11 (2019) 229–235. https://doi.org/10.30880/ijie.2019.11.05.029.

[15] K. Mohanta, D. Kumar, O. Parkash, Properties and Industrial Applications of Rice husk : A review, Int. J. Emerg. Technol. Adv. Eng. 2 (2012) 86–90.

[16] A. Pattnayak, N. Madhu, A.S. Panda, M.K. Sahoo, K. Mohanta, A Comparative study on mechanical properties of Al-SiO2 composites fabricated using rice husk silica in crystalline and amorphous form as reinforcement, Mater. Today Proc. 5 (2018) 8184–8192. https://doi.org/10.1016/j.matpr.2017.11.507.

[17] T.G. Korotkova, S.J. Ksandopulo, A.P. Donenko, S.A. Bushumov, A.S. Danilchenko, Physical properties and chemical composition of the rice husk and dust, Orient. J. Chem. 32 (2016) 3213–3219. https://doi.org/10.13005/ojc/320644.

[18] R.A. Bakar, R. Yahya, S.N. Gan, Production of High Purity Amorphous Silica from Rice Husk, Procedia Chem. 19 (2016) 189–195. https://doi.org/10.1016/j.proche.2016.03.092.

[19] M. Sarangi, P. Nayak, T.N. Tiwari, Effect of temperature on nano-crystalline silica and carbon composites obtained from rice-husk ash, Compos. Part B Eng. 42 (2011) 1994–1998. https://doi.org/10.1016/j.compositesb.2011.05.026.

[20] J. James, M.S. Rao, Silica from rice husk through thermal decomposition, Thermochim. Acta. 97 (1986) 329–336. https://doi.org/10.1016/0040-6031(86)87035-6.

[21] A. Rivas, G. Vera, V. Palacios, A. Rigail, M.H. Cornejo Martínez, Characterization of Rice Husk and the Crystallization Process of Amorphous Silica from Rice Husk Ash, (2016). https://doi.org/10.18687/laccei2016.1.1.093.

[22] A.L. Rivas, G. Vera, V. Palacios, M. Cornejo, A. Rigail, G. Solórzano, Phase Transformation of Amorphous Rice Husk Silica, Front. Mater. Process. Appl. Res. Technol. (2018) 17–26. https://doi.org/10.1007/978-981-10-4819-7_2.

[23] N.E. Udoye, O.J. Nnamba, O.S.I. Fayomi, A.O. Inegbenebor, K.J. Jolayemi, Analysis

on mechanical properties of AA6061/Rice husk ash composites produced through stir casting technique, Mater. Today Proc. 43 (2020) 1415–1420. https://doi.org/10.1016/j.matpr.2020.09.178.

[24] C.M. Gomes, A.L. Garry, E. Freitas, C. Bertoldo, G. Siqueira, Effects of Rice Husk Silica on microstructure and mechanical properties of Magnesium-oxychloride Fiber Cement (MOFC), Constr. Build. Mater. 241 (2020). https://doi.org/10.1016/j.conbuildmat.2020.118022.

[25] S. Sarkar, A. Bhirangi, J. Mathew, R. Oyyaravelu, P. Kuppan, A.S.S. Balan, Fabrication characteristics and mechanical behavior of Rice Husk Ash-Silicon Carbide reinforced Al-6061 alloy matrix hybrid composite, Mater. Today Proc. 5 (2018) 12706–12718. https://doi.org/10.1016/j.matpr.2018.02.254.

[26] Mechanical and thermal behavior of kaolin_rice-husk ash matrix composites reinforced with corrugated steel fibers.pdf, (n.d.).

[27] Mechanical strength and microstructure of metakaolin_volcanic ash-based geopolymer composites reinforced with reactive silica from rice husk ash (RHA).pdf, (n.d.).

[28] K.K. Alaneme, K.O. Sanusi, Microstructural characteristics, mechanical and wear behaviour of aluminium matrix hybrid composites reinforced with alumina, rice husk ash and graphite, Eng. Sci. Technol. an Int. J. 18 (2015) 416–422. https://doi.org/10.1016/j.jestch.2015.02.003.

[29] I. Dinaharan, K. Kalaiselvan, E.T. Akinlabi, J.P. Davim, Microstructure and wear characterization of rice husk ash reinforced copper matrix composites prepared using friction stir processing, J. Alloys Compd. 718 (2017) 150–160. https://doi.org/10.1016/j.jallcom.2017.05.117.

[30] K. Mohanta, A. Kumar, O. Parkash, D. Kumar, Processing and properties of low cost macroporous alumina ceramics with tailored porosity and pore size fabricated using rice husk and sucrose, J. Eur. Ceram. Soc. 34 (2014) 2401–2412. https://doi.org/10.1016/j.jeurceramsoc.2014.01.024.

[31] A. Parrillo, G. Sánchez, A. Bologna, Alles, α-Si_3N_4 and Si_2N_2O whiskers from rice husk and industrial rice husk ash. SN Applied Sciences (2021) 3:268. https://doi.org/10.1007/s42452-021-04307-y.

[32] M.F. Zawrah, M.A. Zayed, M.R.K. Ali, Synthesis and characterization of SiC and SiC/Si $_3N_4$ composite nanopowders from waste material, J. Hazard. Mater. 227–228 (2012) 250–256. https://doi.org/10.1016/j.jhazmat.2012.05.048.

[33] I. Dinaharan, K. Kalaiselvan, E.T. Akinlabi, J.P. Davim, Microstructure and wear characterization of rice husk ash reinforced copper matrix composites prepared using friction stir processing, J. Alloys Compd. 718 (2017) 150–160. https://doi.org/10.1016/j.jallcom.2017.05.117.

[34] A.L. Rivas, G. Vera, V. Palacios, M. Cornejo, A. Rigail, G. Solórzano, Phase Transformation of Amorphous Rice Husk Silica, Front. Mater. Process. Appl. Res. Technol. (2018) 17–26. https://doi.org/10.1007/978-981-10-4819-7_2.

[35] M.E. Kjelstadli, Kinetics and Mechanism of Phase Transformations from Quartz to Cristobalite, (2016) 85.

[36] B.I. Ugheoke, O. Mamat, B. Ari-Wahjoedi, Thermal expansion behavior, phase transitions and some physico-mechanical characteristics of fired doped rice husk silica refractory, J. Adv. Ceram. 2 (2013) 79–86. https://doi.org/10.1007/s40145-013-0046-0.

[37] J.P. Nayak, J. Bera, Effect of sintering temperature on phase-formation behavior and Mechanical properties of silica ceramics prepared from rice husk ash, Phase Transitions. 82 (2009) 879–888. https://doi.org/10.1080/01411590903471564.

[38] H. Mao, B. Sundman, Z. Wang, S.K. Saxena, Volumetric properties and phase relations of silica - Thermodynamic assessment, J. Alloys Compd. 327 (2001) 253–262. https://doi.org/10.1016/S0925-8388(01)01465-7.

[39] T. Arahori, T. Suzuki, Transformation of tridymite to cristobalite below 1470° C in silica refractories, J. Mater. Sci. 22 (1987) 2248–2252. https://doi.org/10.1007/BF01132967.

Chapter 6

Microstructural characterization and hydrothermal ageing resistance of RHA-derived amorphous and crystalline silica-doped Alumina toughened Zirconia biocomposite.